

First principles simulations of Li ion migration in materials related to LiPON electrolytes

Y. A. Du¹ and N. A. W. Holzwarth

Department of Physics, Wake Forest University, Winston-Salem, NC 27109, USA

In an effort to understand stability and ionic conduction mechanisms in the LiPON family of solid electrolytes, we have carried out first principles calculations of several related crystalline materials. Simulation results include heats of formation, zone center lattice vibrational modes, and activation energies for Li ion migration. In the course of this work, we discovered new stable crystalline forms of $\text{Li}_2\text{PO}_2\text{N}$, based on the previously known phosphate chain structure of LiPO_3 .

Introduction

The solid state film electrolyte LiPON, developed at Oak Ridge National Laboratory,[1, 2] is the most widely used solid electrolyte for thin film batteries and a number of other related technologies. While commercial LiPON electrolytes are disordered, much can be learned from related crystalline materials in the $\text{Li}_x\text{PO}_y\text{N}_z$ family ($x = 2y + 3z - 5$). By performing “first principles” simulations on these materials, we can determine stable and meta-stable phosphonitride structures and stoichiometries and relate them to mechanisms of Li ion conductivity.

Computational methods

“First principles” simulations were performed by using density functional theory[3, 4] to treat the electrons and the Born-Oppenheimer approximation to treat the atomic positions $\{\mathbf{R}^a\}$, resulting in a determination of the “total energy” $E(\{\mathbf{R}^a\})$ of the system. The local density approximation[5] was used for the exchange-correlation functional. Most of the computations were carried out using the *PWscf* package,[6] but for validation and convenience we used the *abinit*[7] and *pwpaw*[8] packages as well. Visualizations were constructed using the *OpenDX*[9] and *XCrySDEN*[10] software packages.

From restricted optimizations of the total energies $E(\{\mathbf{R}^a\})$ with respect to the atomic positions $\{\mathbf{R}^a\}$, we can determine a variety of properties including: stable and meta-stable structures, lattice vibration modes and frequencies (ν), heats of formation (ΔH), migration energies (E_m) using the “nudged elastic band” method,[11, 12, 13] and energies for interstitial-vacancy pair formation (E_f).

¹Current address: ICAMS, Ruhr-Universität, 44780 Bochum, Germany

In terms of the electrolyte properties, the connection between simulation and experiment is most easily made through the Arrhenius relation for ionic conduction (σ) as a function of temperature (T):

$$\sigma \cdot T = \underbrace{K}_{\text{Constant}} e^{-E_A/kT}, \quad (1)$$

where k denotes the Boltzmann constant. The constant K is independent of temperature, but does depend on the properties of the electrolyte. For crystalline materials the activation energy E_A is related to the migration energy E_m and the “formation” energy E_f of a vacancy and interstitial ion in an otherwise perfect lattice:

$$E_A = \underbrace{E_m}_{\text{Migration}} + \frac{1}{2} \underbrace{E_f}_{\text{Formation}}. \quad (2)$$

For disordered materials which have a temperature independent concentration of mobile ions, the activation energy is equal to the migration energy:

$$E_A = \underbrace{E_m}_{\text{Migration}}. \quad (3)$$

In order to check the accuracy of our simulations, we can compare our lattice vibrational modes with experiment. In figures 1 and 2 we show comparison of Raman spectral frequencies for γ -Li₃PO₄ [14] and infrared spectral frequencies for α -P₃PN₅, respectively. These comparisons show generally good agreement between simulation and experiment, particularly for the higher frequency modes.

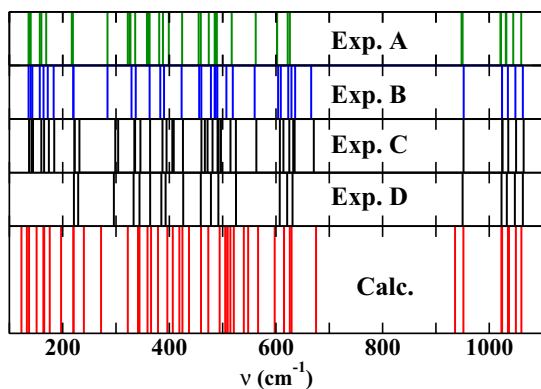


Figure 1: Calculated Raman spectra of γ -Li₃PO₄ (bottom panel) compared with experimental results: Exp. A (room temperature) [15], Exp. B (room temperature) and Exp. C (liquid nitrogen temperature) [16], and Exp. D (liquid nitrogen temperature) [17].

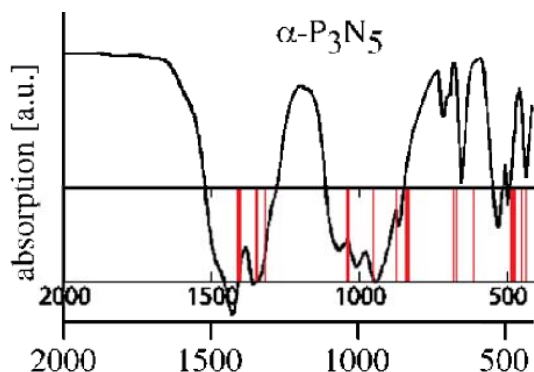


Figure 2: Calculated infrared modes of α -P₃PN₅ (center strip) compared with transmittance infrared spectrum scanned from Ref. [18].

Overview of then LiPON family of materials

In order to systematize the current state of understanding of the crystalline members of the family, it is helpful to visualize a quaternary phase diagram of known materials reported in the literature together with new stable and meta-stable materials predicted by computer simulation as shown in Fig. 3

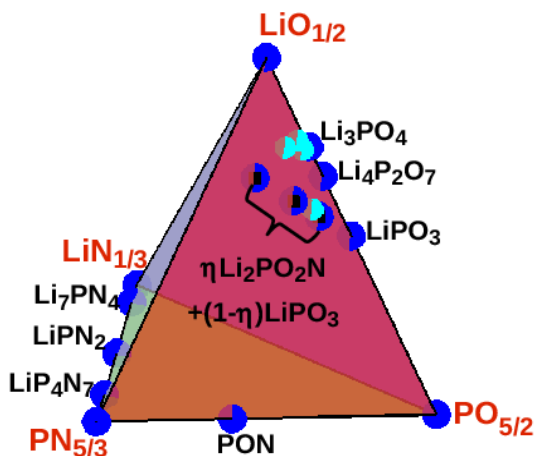


Figure 3: Quaternary composition diagram for $\text{Li}_x\text{PO}_y\text{N}_z$ with corners of the tetrahedron indicating the starting materials of $\text{LiO}_{1/2}$, $\text{LiN}_{1/3}$, $\text{PO}_{5/2}$, and $\text{PN}_{5/3}$. Symbols denote natural and synthetic crystalline materials (\bullet), LiPON thin film materials (\circ), and computer simulated idealized phosphate chain structure materials (\blacksquare).

Each of the labels given beside the tetrahedron in Fig. 3 represents an experimentally determined crystal material in the $\text{Li}_x\text{PO}_y\text{N}_z$ family. We have carried out simulations for most of these materials.[19] The present paper focuses attention on the materials based on phosphate chain structures.

Simulations of materials based on the phosphate chain material LiPO_3

Crystalline LiPO_3 can be prepared from a $\text{Li}_2\text{O-P}_2\text{O}_5$ glass by heating it to the crystallization temperature of 486°C . [20] It is known to have the space group symmetry $P2/c$ [21] with a unit cell of 100 atoms. Table 1 compares our calculated lattice parameters with those determined from X-ray analysis. The monoclinic structure is visualized with ball and stick diagrams in two different perspectives in Fig. 4.

Table 1: Lattice parameters (in \AA) for LiPO_3 comparing calculated results with experimental results of Ref. [21].

	a	b	c	β
Cal.	13.00	5.30	16.31	98.8°
Exp.	13.074	5.4068	16.452	99.00°

An important question related to LiPON materials is the role of N in the lattice structures. Qualitatively, N is known to “strengthen” phosphate glasses. From our previous studies,[22] we know that an O can be replaced with N plus an additional Li. We also know that it is energetically favorable for a N ion to replace an O ion on a site which bridges two

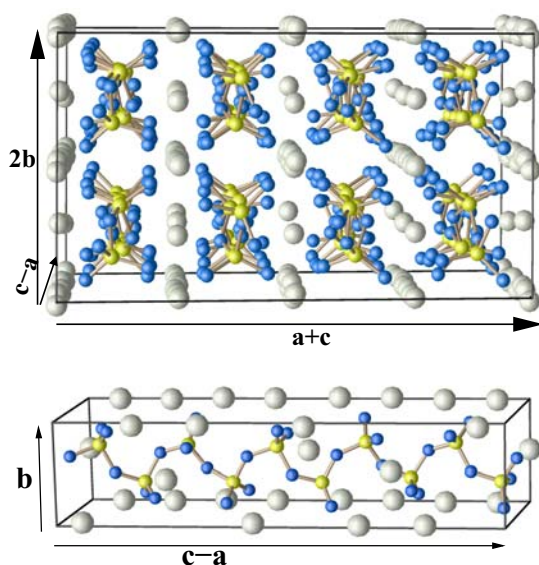


Figure 4: Two views of the $P2/c$ structure of LiPO_3 ; top diagram showing the chain direction perpendicular to the plane of the diagram and bottom diagram showing a view of a single chain. The balls are given with $\bullet = \text{Li}$, $\bullet = \text{P}$, $\bullet = \text{O}$.

phosphate groups rather than replacing an O ion tetrahedrally coordinated with phosphorus. Therefore, we modified the 100 atom unit crystal of LiPO_3 by replacing the 20 bridge bonding oxygens with nitrogens and adding 20 additional Li atoms. The optimized geometry of this modified crystal had a surprisingly simple structure with space group $Pbcm$ shown in Fig. 5. From this figure, it is evident that the Li ions are stabilized by proximity to both O and N interactions.

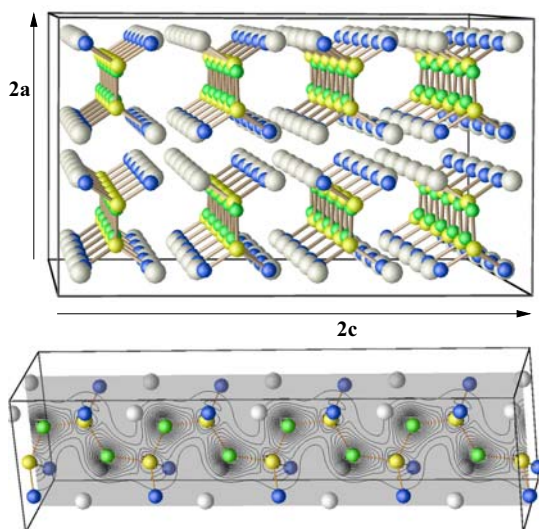


Figure 5: Two views of the $Pbcm$ structure of $\text{Li}_2\text{PO}_2\text{N}$; top diagram showing the chain direction perpendicular to the plane of the diagram and bottom diagram showing a view of a single chain. The balls are given with $\bullet = \text{Li}$, $\bullet = \text{P}$, $\bullet = \text{O}$, $\bullet = \text{N}$. In the lower figure, a contour diagram of valence electron charge density is plotted in a plane containing the phosphonitride backbone.

Having created this new material, we can then ask the question of whether the structural transformation is reversible. In the simulations, we can start from the $Pbcm$ structure of $\text{Li}_2\text{PO}_2\text{N}$ and try to replace the N's with O and to remove 20 Li ions in order to reform the original LiPO_3 structure. Not surprisingly, this is difficult since there are many meta-stable structures of LiPO_3 . In fact it is relatively easy to find a meta-stable $Pbcm$ structure of LiPO_3 shown in Fig. 6. Comparing the s_1 structures shown in Figs. 5 and 6, we see that in $\text{Li}_2\text{PO}_2\text{N}$ there is a Li ion associated with each O site, while in LiPO_3 the Li ions are shared between phosphate chains.

In fact, there are many meta stable structures for both $\text{Li}_2\text{PO}_2\text{N}$ and LiPO_3 . For example,

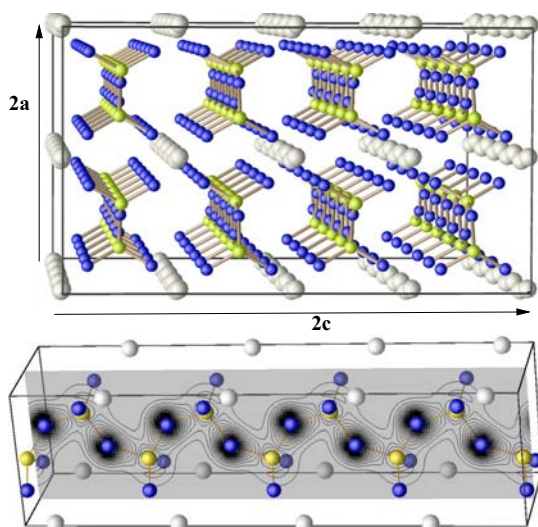


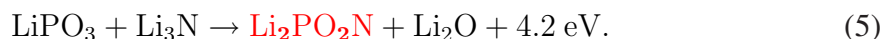
Figure 6: Two views of $Pbcm$ structure of LiPO_3 ; top diagram showing the chain direction perpendicular to the plane of the diagram and bottom diagram showing a view of a single chain. The balls are given with $\bullet = \text{Li}$, $\bullet = \text{P}$, $\bullet = \text{O}$. In the lower figure, a contour diagram of valence electron charge density is plotted in a plane containing the phosphate backbone.

the $Pbcm$ structure contains two orientationally inequivalent chains per unit cell. By rotating one of the chains by 180° about an axis perpendicular to the plane of the phosphonitride chain, it is possible to find a very similar structure with $Aem2$ symmetry. Table 2 summarizes some of the simulation results in terms of formation energies and other parameters.

Table 2: Comparison of different structural forms of LiPO_3 and $\text{Li}_2\text{PO}_2\text{N}$ in terms of their heats of formation (ΔH_{cal}) and volumes \mathcal{V}_{cal} (per formula unit).

Material	Structure	ΔH_{cal} (eV)	\mathcal{V}_{cal} (\AA^3)
LiPO_3	$P2/c$ [#13]	-12.80	56
$s_1\text{-LiPO}_3$	$Pbcm$ [#57]	-12.73	58
$s_2\text{-LiPO}_3$	$Aem2$ [#39]	-12.73	58
$s_3\text{-LiPO}_3$	$Pmc2_1$ [#26]	-12.70	67
$s_1\text{-Li}_2\text{PO}_2\text{N}$	$Pbcm$ [#57]	-12.42	57
$s_2\text{-Li}_2\text{PO}_2\text{N}$	$Aem2$ [#39]	-12.45	57
$s_3\text{-Li}_2\text{PO}_2\text{N}$	$Pmc2_1$ [#26]	-12.08	66

From this table we can see that the synthetic forms of LiPO_3 have higher energy than the natural crystal, so it may not be possible to physically realize those structures. On the other hand, we believe that it should be possible to synthesize either or both of the $Pbcm$ and $Aem2$ forms of $\text{Li}_2\text{PO}_2\text{N}$. The calculation results allow us to predict the following possible exothermic reaction pathways.



It is also interesting to compare the zone center lattice vibrational spectra for these materials as shown in Fig. 7. These figures show that the $P2/c$ structure of LiPO_3 has a dense spectrum of vibrational modes which is not surprising for a material with 100 atoms in the unit cell. The meta-stable $s_1\text{-LiPO}_3$ structure ($Pbcm$) has roughly one-fourth as many

modes covering a similar range of frequencies. For all three materials, the modes having appreciable Li ion motion have generally low frequency ($\nu < 800 \text{ cm}^{-1}$). The highest frequency modes involve both motions of the O or N bridging site and of the tetrahedral oxygens. For $s_1\text{-Li}_2\text{PO}_2\text{N}$, the highest frequency modes are lower by 100-200 (cm^{-1}) compared with corresponding modes in the LiPO_3 materials.

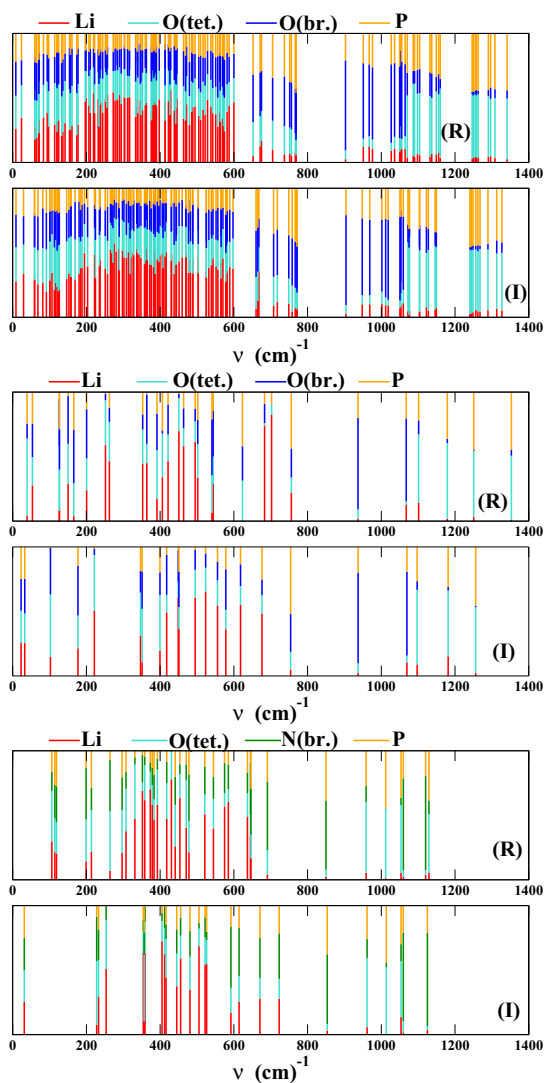


Figure 7: Calculated zone center lattice frequencies ν in units of (cm^{-1}), presenting Raman active (R) and infrared active (I) in separate plots. Results are given for $P2/c \text{ LiPO}_3$ (top) $Pbcm \text{ LiPO}_3$ (middle) and $Pbcm \text{ Li}_2\text{PO}_2\text{N}$ (bottom). In each plot modes are further analyzed in terms of the amplitudes of motion for each type of atom, normalized to unity as indicated in the figure legends.

Using the “nudged elastic band” method,[11, 12, 13] we estimated the migration energies for several vacancy paths and a representative interstitial path in $P2/c$ crystals of LiPO_3 . The vacancy migration paths, indicated with the arrows in the structural model shown in Fig. 8, were simulated in a supercell containing 200 atoms. There are two inequivalent paths along the (c- a) axes, parallel to the phosphate chains which we call the “majority” rows. Each of these paths each containing 4 meta-stable vacancy sites and have similar variations in their minimal energy paths (E_{path}). We also simulated a vacancy migration path along the b axis, corresponding to the migration of a Li ion vacancy between a “minority” row and a vacancy in a “majority” row. The the corresponding energy path diagrams are shown in the right side of Fig. 8. The zero of energy for E_{path} was taken to be the lowest meta-stable vacancy energy, which happens to occur in a minority row. The esti-

Table 3: Summary of calculated migration energies for mobile Li ions in $P2/c$ LiPO_3 for vacancy paths indicated in Fig. 8 and for a representative interstitial path.

	Vacancy			Interstitial
	(c-a)-1	(c-a)-2	(b)	
E_m	0.6	0.6	0.7	0.7

mated values of E_m (migration energies) are summarized in Table 3, including those for the vacancy mechanisms shown in Fig. 8 as well as a representative interstitial path involving Li ions in a minority row migrating along the chain direction. Interestingly, the Li ion vacancy migration energies for the phosphate chain material $P2/c$ LiPO_3 reported here are comparable to vacancy migration energies found for Li_3PO_4 reported in earlier work,[14] even though the phosphate structures are quite different. Li_3PO_4 has no phosphate chains; rather it is characterized by isolated $[\text{PO}_4]^{-3}$ groups. By contrast, for Li_3PO_4 , we found a lower energy migration process with an interstitial mechanism. A comparable low energy interstitial mechanism for Li ion migration has not yet been found for $P2/c$ LiPO_3 .

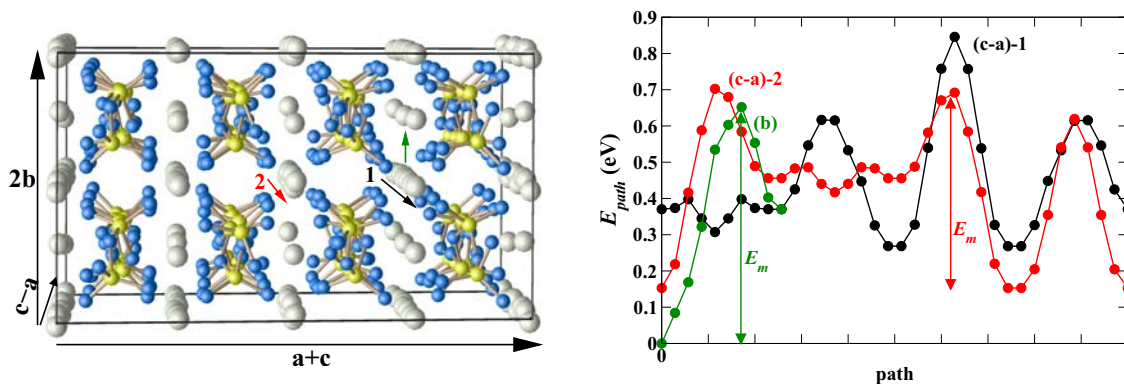


Figure 8: Left: Paths for Li ion vacancy diffusion in $P2/c$ LiPO_3 indicated with arrows. Right: Energy path diagram for indicated paths. Horizontal axis is related to migration distance.

Summary of results

Table 4 presents a comparison of measured activation energies for several members of the LiPON family compared with calculated migration energies E_m in crystalline materials and formation energies E_f for the creation of a pair of vacancy and interstitial in an otherwise perfect lattice. For all of the calculated crystalline materials, the activation energies are dominated by the formation energies E_f . In addition to the results for $P2/c$ LiPO_3 described in this paper, results for γ - Li_3PO_4 from earlier work[14] and unpublished results for LiPN_2 are also presented. Except for the case of LiPN_2 , [26] the agreement between the calculated and measured activation energies of crystalline materials is quite good. In addition, we have calculated the migration energy and activation energy for the new predicted material s_1 - $\text{Li}_2\text{PO}_2\text{N}$. Our results indicate that s_1 - $\text{Li}_2\text{PO}_2\text{N}$ has migration energies and activation energies comparable to Li_3PO_4 and LiPO_3 . For this structure, the presence of N does not seem to enhance the Li ion mobility, perhaps because the Li ions are stabilized by both O and N interactions. On the other hand, the s_1 and s_2 structures of $\text{Li}_2\text{PO}_2\text{N}$

Table 4: Measured activation energies E_A^{exp} compared with calculated migration energies for vacancy (E_m^{cal} (vac.)) and interstitial (E_m^{cal} (int.)) mechanisms and vacancy-interstitial formation energies (E_f^{cal}) for crystalline materials. From these values, the activation energies (E_A^{cal}) are determined from Eq. (2). All energies are given in eV.

Material	Form	E_A^{exp}	E_m^{cal} (vac.)	E_m^{cal} (int.)	E_f^{cal}	E_A^{cal}
γ -Li ₃ PO ₄	single crystal	1.23, 1.14 [23]	0.7, 0.7	0.4, 0.3	1.7	1.3, 1.1
Li _{2.88} PO _{3.73} N _{0.14}	poly cryst.	0.97 [24]				
Li _{3.3} PO _{3.9} N _{0.17}	amorphous	0.56 [24]				
Li _{1.35} PO _{2.99} N _{0.13}	amorphous	0.60 [25]				
LiPO ₃	poly cryst.	1.4 [20]	0.6, 0.7	0.7	1.2	1.1, 1.2
LiPO ₃	amorphous	0.76-1.2 [20]				
<i>s</i> ₁ -Li ₂ PO ₂ N	single crystal		0.5, 0.6		1.7	1.3, 1.5
LiPN ₂	poly cryst.	0.6 [26]	0.4		2.5	1.7
Li ₇ PN ₄	poly cryst.	0.5 [26]				

are undoubtedly highly symmetric and stable. If it is possible to synthesize and analyze *s*₁-Li₂PO₂N and/or the very similar *s*₂-Li₂PO₂N, it will provide a valuable benchmark for understanding local structures and mechanisms in LiPON materials.

In summary, we have presented part of our work on a broad study of crystalline materials related to LiPON solid electrolyte materials. Estimating the migration energy of Li ion vacancies in these materials we have found values in the range of $0.4 \leq E_m \leq 0.7$ eV. If one assumes that the LiPON films have temperature independent populations of mobile ions and environments similar to those found in the crystalline materials, it is perhaps not surprising that our calculated migrations are similar to activation energies measured for LiPON films.[1, 24, 25]

An unexpected, but nevertheless intriguing result of our study of chain structure materials and the possible role of N replacing O, is the prediction of are two highly symmetric crystalline forms of Li₂PO₂N which we have called the *s*₁- and *s*₂- structures with the *Pbcm* and *Aem2* space groups, respectively. We would like to challenge our experimental colleagues to prove (or disprove) these predictions.

Acknowledgments

This work was supported by NSF grants DMR-0427055 and 0705239 and by The Wake Forest University DEAC computer cluster.

Bibliography

- [1] J. B. Bates, *et al.*, *Solid State Ionics* **53–56**, 647 (1992).
- [2] N. J. Dudney, *Interface* **17**, 44 (2008).
- [3] P. Hohenberg, W. Kohn, *Physical Review* **136**, B864 (1964).
- [4] W. Kohn, L. J. Sham, *Physical Review* **140**, A1133 (1965).
- [5] J. P. Perdew, Y. Wang, *Phys. Rev. B* **45**, 13244 (1992).
- [6] P. Giannozzi, *et al.*, *J. Phys.: Condens. Matter* **21**, 394402 (19pp) (2009). Available from the website <http://www.quantum-espresso.org>.
- [7] X. Gonze, *et al.*, *Zeit. Kristallogr.* **220**, 558 (2005). Available from the website <http://www.abinit.org>.
- [8] A. R. Tackett, N. A. W. Holzwarth, G. E. Matthews, *Computer Physics Communications* **135**, 348 (2001). Available from the website <http://pwpaw.wfu.edu>.
- [9] OpenDX – The Open Source Software Project Based on IBM’s Visualization Data Explorer – is available from the web site <http://www.opendx.org>.
- [10] A. Kokalj, *Journal of Molecular Graphics and Modelling* **17**, 176 (1999).
- [11] H. Jónsson, G. Mills, K. W. Jacobsen, *Classical and Quantum Dynamics in Condensed Phase Simulations*, B. J. Berne, G. Ciccotti, D. F. Coker, eds. (World Scientific, Singapore, 1998), pp. 385–404.
- [12] G. Henkelman, B. P. Uberuaga, H. Jónsson, *J. Chem. Phys.* **113**, 9901 (2000).
- [13] G. Henkelman, H. Jónsson, *J. Chem. Phys.* **113**, 9978 (2000).
- [14] Y. A. Du, N. A. W. Holzwarth, *Phys. Rev. B* **76**, 174302/1 (2007).
- [15] B. N. Mavrin, V. V. Asonov, V. V. Fomichev, A. K. Ivanov-Shitz, V. V. Kireev, *Journal of Experimental and Theoretical Physics* **96**, 53 (2003).
- [16] F. Harbach, F. Fischer, *Phys. Stat. Sol. (b)* **66**, 237 (1974).
- [17] L. Popović, B. Manoun, D. de Wall, M. K. Nieuwoudt, J. D. Comins, *Journal of Raman Spectroscopy* **34**, 77 (2003).
- [18] P. Kroll, W. Schnick, *Chem. Eur. J.* **8**, 3530 (2002).
- [19] Y. A. Du, N. A. W. Holzwarth. To be published.

- [20] B. K. Money, K. Hariharan, *Applied Physics A* **88**, 647 (2007).
- [21] E. V. Murashova, N. N. Chudinova, *Crystallography Reports* **46**, 942 (2001).
- [22] Y. A. Du, N. A. W. Holzwarth, *Phys. Rev. B* **78**, 174301 (2008).
- [23] A. K. Ivanov-Shitz, V. V. Kireev, O. K. Mel'nikov, L. N. Demainets, *Crystallography Reports* **46**, 864 (2001).
- [24] B. Wang, B. C. Chakoumakos, B. C. Sales, B. S. Kwak, J. B. Bates, *Journal of Solid State Chemistry* **115**, 313 (1995).
- [25] F. Muñoz, *et al.*, *Solid State Ionics* **179**, 574 (2008).
- [26] W. Schnick, J. Luecke, *Solid State Ionics* **38**, 271 (1990).